

Relative Stability and Local Curvature Analysis in Carbon Nanotori

Chern Chuang,¹ Jie Guan,² David Witalka,² Zhen Zhu,² Bih-Yaw Jin,³ and David Tománek^{2,*}

¹*Department of Chemistry, Massachusetts Institute of Technology, Cambridge, MA 02139, USA*

²*Physics and Astronomy Department, Michigan State University, East Lansing, Michigan 48824, USA*

³*Department of Chemistry and Center for Emerging Material and Advanced Devices,
National Taiwan University, Taipei 10617, Taiwan*

(Dated: November 16, 2021)

We introduce a concise formalism to characterize nanometer-sized tori based on carbon nanotubes and to determine their stability by combining *ab initio* density functional calculations with a continuum elasticity theory approach that requires only shape information. We find that the high strain energy in nanotori containing only hexagonal rings is significantly reduced in nanotori containing also other polygons. Our approach allows to determine local curvature and link it to local strain energy, which is correlated with local stability and chemical reactivity.

PACS numbers: 61.48.De, 68.55.ap, 61.46.-w, 81.05.ub

INTRODUCTION

The past three decades witnessed an unprecedented progress in the synthesis and use of nanostructures consisting of elemental carbon ranging from fullerenes to carbon nanotubes and graphene¹⁻⁴. Due to the stiffness of the σ bonding network and the delocalization of the π electrons in these systems, the structure-property relationships are highly nontrivial, as presence of local atomic defects is known to affect physical properties on the mesoscopic length scale⁵. In this regard, owing to their peculiar geometry and topology⁶, carbon nanotori based on single-wall carbon nanotubes serve as an excellent test ground for studying such effects. To name just a few, reversible elastic deformation of carbon nanotori has been predicted⁷ and experimentally identified⁸, implying potential application in force-sensing devices. Gigantic paramagnetic response⁹, persistent currents¹⁰⁻¹² and even molecular anapole moments¹³ have been predicted for specific nanotorus geometries. Also, the intricate shape of carbon nanotori can be exploited in the context of host-guest chemistry and physics; for example, megahertz oscillations of a nanotorus mounted on a nanotube¹⁴ and metal-encapsulated nanotori with net magnetic moment¹⁵ have been predicted. A crucial prerequisite to realize these interesting physical properties is to establish, to what degree the postulated toroidal nanostructures are stable mechanically and thermally.

Here we study the stability of carbon nanotori formed conceptually by bending a finite-length single-wall carbon nanotube (CNT) and connecting its ends seamlessly. Such a nanotorus can then be characterized the chiral index¹⁶ (n, m) of the nanotube and number of primitive unit cells along the perimeter. We will refer to this family of nanotori, which contain only hexagonal rings, as to *polyhex* nanotori. It is known that presence of non-hexagonal rings, such as 5-7 pairs, induces a bend in a straight nanotube. In the following, we will refer to the family of nanotori that contain also non-hexagonal rings as to *polygonal* nanotori. We will demonstrate that a continuum elasticity theory approach¹⁷, which requires only

shape information, is capable of estimating not only the global stability, but also local strain with a precision approaching that of *ab initio* density functional calculations at a small fraction of the computational cost.

Our manuscript is organized as follows. In the next section we outline the computational techniques used in our study. Next we summarize the characteristics of different nanotori families. Then, we analyze and obtain analytical expressions for the in-plane and out-of-plane contributions to the elastic energy of polyhex nanotori. In the following Section, we will present a general overview of the elastic energy for polygonal nanotori. Next we will discuss the distributions of curvature and elastic energy on polygonal nanotori, and correlate them to the relative positions of the non-hexagonal rings in the systems. This is followed by the asymptotic analysis of three families of polygonal nanotori with varying shape parameters, including changing rotational symmetry, the lateral torus size normal to the axis and the torus height along the axis.

COMPUTATIONAL TECHNIQUES

Our main computational approach is based on continuum elasticity theory, which proved useful in evaluating the strain energy in fullerenes, nanotubes and schwarzites with respect to a planar graphene monolayer and corresponding stability differences¹⁷.

In systems with no frustration, where areas of Voronoi polygons associated with individual atoms are at the optimum value, the in-plane strain energy is very small. This proved to be the case in carbon nanotubes¹⁷ and we expect it to hold also in the related nanotori. Neglecting the in-plane component of strain, the stability of nanotori could be analyzed in the inextensional limit of the mechanical theory of a membrane¹⁸, where the elastic energy is dominated by its out-of-plane component.

The out-of-plane strain or curvature energy of a given

closed membrane can be expressed as

$$\Delta E_c = D \int_S dA [2k^2 - (1 - \alpha)G], \quad (1)$$

where D is the flexural rigidity, α the Poisson ratio, k the local mean curvature, G the local Gaussian curvature, and the integration is carried out over the surface S of the membrane. If instead of the general shape we know the precise atomic locations from either diffraction experiments or *ab initio* calculations, we can rather use the discretized version of Eq. (1),

$$\Delta E_c \approx A_0 D \sum_i [2k_i^2 - (1 - \alpha)G_i]. \quad (2)$$

Here, A_0 is the area per atom, k_i the local mean curvature and G_i the local Gaussian curvature at atom site i . The summation covers all atoms of the torus. For structures comprising of more than one element, the quantity A_0 may vary and needs to be taken inside of the summation. Alongside with this expression, accurate ways to estimate k_i and G_i based on the *local geometry* in the vicinity of site i have been proposed recently¹⁷, which have been validated by *ab initio* density functional calculations. Even though this method relies on the knowledge of the molecular geometry, it has been shown that even inexpensive classical force fields serve the purpose of structure optimization surprisingly well when compared against state-of-the-art *ab initio* calculations for a wide range of graphitic structures^{17,19}.

The total in-plane strain energy can be estimated in the continuum model from an integral over the entire surface area A ,

$$\Delta E_s = \oint_A \epsilon(\sigma) dA, \quad (3)$$

where $\epsilon(\sigma)$ is the energy cost per area subject to strain σ . For specific, small strains, $\epsilon(\sigma)$ may be presented as a harmonic function of the strain σ , with the proper coefficient taken either from experimental data or from *ab initio* calculations.

Selected results based on continuum elasticity theory are validated by *ab initio* calculations in the framework of density functional theory (DFT), as implemented in the SIESTA code.²⁰ We use the local density approximation^{21,22} to describe exchange and correlation in the system, norm-conserving Troullier-Martins pseudopotentials²³, and a double- ζ basis including polarization orbitals. In the reference system, we sample the 2D Brillouin zone of graphene by 16×16 k -points.²⁴ The small Brillouin zones of isolated nanotori are sampled by only 1 k -point. We use a mesh cutoff energy of 180 Ry to determine the self-consistent charge density, which provides precision in total energy of $\lesssim 2$ meV/atom. All geometries are optimized using the conjugate gradient method,²⁵ until none of the residual Hellmann-Feynman forces exceeds 10^{-2} eV/Å.



FIG. 1. (Color online) Atomic structure of (a) a polyhex nanotorus with only hexagons and (b) a polygonal nanotorus containing non-hexagonal rings. (c) A model of a perfect torus with major radius R and minor radius r . θ is the longitudinal angle and ϕ is the azimuthal angle. The yellow shading in (a) and (b) indicates specific polygons in the nanotori.

NANOTORUS CHARACTERISTICS

Due to the extreme flexural stiffness of straight CNTs^{26,27}, it is expected that the number of carbon atoms of a stable polyhex nanotorus should be at least on the order of 10^5 . An example of a polyhex nanotorus containing 400 carbon atoms is shown in Fig. 1(a). For the two shaded hexagons located in the inner and the outer rims of the nanotorus, it is obvious that the in-plane strain energy is inversely proportional to the size of the nanotori. This will be addressed in detail in the following section.

In contrast to polyhex nanotori, there has been considerable effort in describing the second family of polygonal nanotori, which also contain non-hexagonal rings. Due to the requirement of trivalency of sp^2 carbon atoms and the Euler's theorem, the number of non-hexagonal rings on a general closed surface is constrained by

$$\sum_{m>2} (6 - m)N_m = 6\chi, \quad (4)$$

where N_m is the number of the m -gonal rings and χ is the Euler characteristic of the closed surface in question. For a torus, we have $\chi = 0$. Thus, if we restrict ourselves to polygonal nanotori having only pentagons, hexagons, and heptagons, the number of pentagons (N_5) must equal that of heptagons (N_7). Apart from this simple equation, there are many more combinatorial and geometrical constraints for a stable polygonal carbon nanotorus to exist²⁸. The polygonal nanotori covered in this study are restricted to those of high symmetry (D_{nd} or D_{nh} point group) and a smaller number of atoms (< 60 atoms per rotational unit cell). One such polygonal nanotorus is shown in Fig. 1(b), a representative pentagon on the outer and a heptagon on the inner side of the nanotorus are highlighted. As suggested before, the existence of these non-hexagonal rings induces natural bending and thus drastically reduces the in-plane strain energy.

ELASTIC ENERGY IN NANOTORI

As suggested above, the elastic energy within carbon nanotori can be divided into two parts: in-plane and

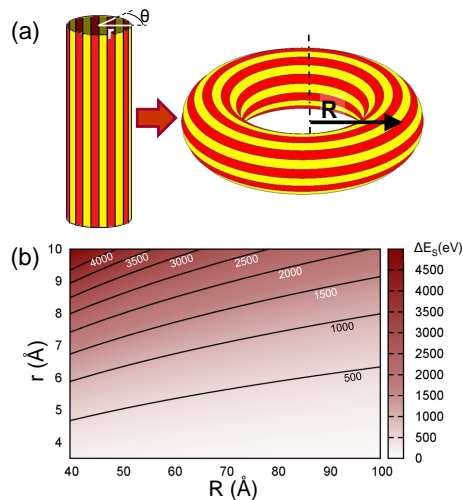


FIG. 2. (Color online) (a) Schematic of a striped nanotube (left), which is bent to a nanotorus (right). (b) Contour plot representing the in-plane strain energy $\Delta E_s(R, r)$ according to Eq. (9).

out-of-plane strain energy. The in-plane strain originates from an uneven distribution of atomic area densities as compared to graphene at equilibrium. This is most obvious in polyhex nanotori, where hexagons along the outer perimeter are stretched and those along the inner perimeter are compressed, as seen in Fig. 1(a). The out-of-plane strain energy is associated with forming any curved surface of an intrinsically flat material.

In this section we examine these two contributions to the elastic energy of nanotori. In particular, we will provide and analyze analytical expressions for polyhex nanotori without buckling²⁹. For polygonal nanotori, we will show that the contribution from the in-plane strain is negligible, similar to the case of small fullerenes¹⁷.

In-Plane Strain Energy in Polyhex Nanotori

Points on the surface of a perfect parametric torus are described by

$$\begin{cases} x = (R - r \cos \theta) \cos \phi, \\ y = (R - r \cos \theta) \sin \phi, \\ z = r \sin \theta. \end{cases} \quad (5)$$

Here and in Fig. 1(c), R is the major and r the minor radius, θ the zenith angle, and ϕ the azimuthal angle. Note that $R > r$ is required for a normal ring torus without self-intersection. A polyhex nanotorus, shown in Fig. 1(a), can be constructed by rolling up a finite CNT and connecting the two ends together, as indicated in Fig. 2(a). The major radius R of the polyhex nanotorus can be approximated by the length of the original nanotube divided by 2π . In this case, the area density of atoms is smaller than the average along the outer perimeter of the torus, characterized by $\pi/2 < \theta < 3\pi/2$, and

larger along the inner perimeter. Obviously, the in-plane strain will be negligible in comparison to the out-of-plane strain if $R \gg r$. Should this not be the case, then the in-plane strain energy will be important, as it describes the significant distortion of hexagonal rings along the inner and the outer perimeters of a polyhex nanotorus, which are highlighted in Fig. 1(a).

Here we present a simple estimation of the in-plane strain energy for polyhex nanotori without buckling. As shown in Fig. 2(a), a CNT can be seen as parallel narrow strips or nanoribbons of equal length $2\pi R$ that are connected side-by-side. After the CNT is deformed to a nanotorus, the strips on the inside of the nanotorus are compressed and the strips on the outside are stretched. We further assume that the contributions from all other in-plane distortion modes are negligible. As shown in Fig. 2(a), the width of the strips is $rd\theta$ and the length is $2\pi(R - r \cos \theta)$. The strain σ of the strips can be written as

$$\sigma(\theta) = \frac{2\pi(R - r \cos \theta) - 2\pi R}{2\pi R} = -\frac{r}{R} \cos \theta. \quad (6)$$

The total in-plane strain energy of the nanotorus is just the sum of the strain energies of all the strips,

$$\Delta E_s = \int_0^{2\pi} \epsilon(\sigma) 2\pi(R - r \cos \theta) r d\theta. \quad (7)$$

Here, $\epsilon(\sigma)$ is the energy cost per area of graphene subject to uniaxial strain σ . For sufficiently small strain ($\sigma \lesssim 5\%$), $\epsilon(\sigma)$ is a parabolic function of σ ,

$$\epsilon(\sigma) = c\sigma(\theta)^2 = c\frac{r^2}{R^2} \cos^2 \theta. \quad (8)$$

A fit to graphene data yields the numerical value $c = 9.94 \text{ eV}/\text{\AA}^2$. Substituting Eq. (8) into Eq. (7), we obtain an expression for the total in-plane strain energy of a nanotorus

$$\begin{aligned} \Delta E_s &= \int_0^{2\pi} c \frac{r^2}{R^2} \cos^2 \theta 2\pi(R - r \cos \theta) r d\theta \\ &= 2\pi^2 c \frac{r^3}{R}. \end{aligned} \quad (9)$$

The behavior of $\Delta E_s(R, r)$ in polyhex nanotori is shown in Fig. 2(b). As suggested by Eq. (9), the strain energy is proportional to r^3 and inversely proportional to R . Note that this expression is obtained in the harmonic limit of small strain, which translates into $R \gg r$. Also, we have assumed that the nanotori are ideal and described by Eq. (5). In reality, the cross-section of an elastic nanotorus may deviate from a perfect circle upon relaxation, and buckling may occur along the perimeter. In spite of its limits, this expression provides a concrete estimate of the strain energy of experimentally observed rings based on CNTs³⁰⁻³³. In the reported cases, R is of the order of microns and r of the order of nanometers, so all assumptions in deriving Eq. (9) are justified.

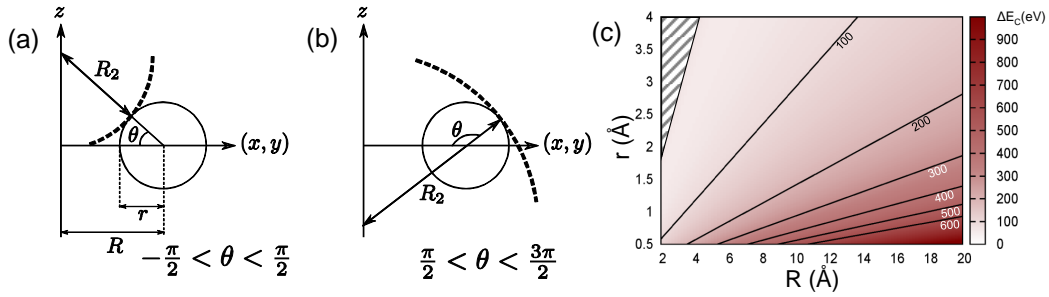


FIG. 3. (Color online) Definition of the principal radius R_2 of a nanotorus in (a) its interior and (b) its exterior part as a function of the zenith angle θ . (c) Contour plot displaying the out-of-plane curvature energy $\Delta E_c(R, r)$ of nanotori according to Eq. (11).

Out-of-Plane Strain Energy in a Perfect Parametric Torus

Besides the in-plane strain, there is also an out-of-plane strain caused by deviation from planarity, which is represented by Eq. (1). For the parametric torus given in Eq. (5), we infer the infinitesimal area dA in Eq. (1) to be $dA = r d\theta \cdot (R - r \cos \theta) d\phi$. Obviously r is one of the principal radii of curvature, which is arbitrarily chosen to be R_1 . The situation is more complicated for R_2 , the other principal radius of curvature. As illustrated in Fig. 3, R_2 is given by

$$R_2(\theta) = \begin{cases} R \sec \theta - r & \text{for } -\frac{\pi}{2} < \theta < \frac{\pi}{2} \\ r - R \sec \theta & \text{for } +\frac{\pi}{2} < \theta < \frac{3\pi}{2} \end{cases}. \quad (10)$$

Clearly, $R_2 \rightarrow \infty$ when $\theta = \pm \frac{\pi}{2}$, which is indeed the case since the torus is tangent to the planes $z = \pm r$.

Now the evaluation of ΔE_c according to Eq. (1) is straightforward. Since the integrand is independent of ϕ , we end up with the expression

$$\begin{aligned} \Delta E_c(R, r) &= \pi D r \int_0^{2\pi} d\theta (R - r \cos \theta) \times \\ &\quad \left(\frac{1}{R_1^2} + \frac{1}{R_2(\theta)^2} + \frac{2\alpha}{R_1 R_2(\theta)} \right) \\ &= 2\pi^2 D \frac{R^2}{r \sqrt{(R+r)(R-r)}}. \end{aligned} \quad (11)$$

In contrast to perfectly spherical fullerenes, where ΔE_c is independent of radius¹⁷, the curvature energy for nanotori depends both on the major radius R and the minor radius r . The out-of-plane curvature energy $\Delta E_c(R, r)$ of carbon nanotori is presented in Fig. 3(c).

We find that the curvature energy does not depend on the Poisson ratio α , a result from the Gauss-Bonnet theorem which states the Gaussian curvature integrated over a closed surface equals the Euler characteristic (χ) of the surface times 2π . Since $\chi = 0$ for nanotori or any tubular structures, ΔE_c does not depend on α . Note that the $1/\sqrt{R-r}$ term in the expression diverges at $R = r$, corresponding to a horn torus, and becomes imaginary for $R < r$, representing spindle nanotori with self-

intersection in the center. In addition, taking the limit of $R \rightarrow \infty$, this expression reduces to the curvature energy of a straight cylinder of length $l = 2\pi R$,

$$\Delta E_c = \frac{\pi D l}{r}. \quad (12)$$

Also, by setting the derivative of ΔE_c with respect to R to zero, one obtains the minimal torus curvature energy of $\Delta E_c = 4\pi^2 D$ for $R = \sqrt{2}r$, as also reported previously^{34,35}.

As mentioned before, for polyhex nanotori described by Eq. (5) and $R \gg r$, the in-plane strain energy can be adequately quantified by Eq. (9) and the out-of-plane strain energy by Eq. (12). Taking polyhex nanotori constructed from (10,10) CNTs with $r = 7 \text{ \AA}$ as an example, the constraint on the major radius R for the harmonic approximation in Eq. (8) to hold is estimated to be $R \gtrsim 150 \text{ \AA}$. For $R = 150 \text{ \AA}$ we find that the in-plane strain energy $\Delta E_s = 450 \text{ eV}$ and the out-of-plane strain energy $\Delta E_c = 600 \text{ eV}$ are of the same order. On the other hand, the majority of rings³⁶ synthesized by ultrasonic wave treatment of CNTs in solution has $R = 3500 \text{ \AA}$. In those rings, the contribution from the in-plane strain, $\Delta E_s = 20 \text{ eV}$, is negligible in comparison with the out-of-plane strain of $\Delta E_c = 1.4 \times 10^4 \text{ eV}$.

Strain Energy in Polygonal Nanotori

In general, the shape of a polygonal nanotorus deviates from that of a perfect parametric torus due to the presence of non-hexagonal defects in a hexagonal network. The largest changes in the curvature occur near individual non-hexagonal defects, and often there are relatively flat segments in-between the defects. Consequently, the analytical expression in Eq. (11) should only be used as a very approximate way to estimate the strain energy of a polygonal nanotorus that is roughly characterized by a set of effective torus radii (R, r). For a quantitatively better energy estimate, we must use the discretized version of Eq. (1), Eq. (2), that takes into account the specific shape of a carbon nanotorus. As mentioned previously,

we first obtain the molecular geometry from the classical Keating force field¹⁹.

Once the optimum geometry is established, the local mean curvature k_i and the local Gaussian curvature G_i are determined everywhere and substituted into Eq. (2). The results of this methodology to a subset of 22 polygonal nanotori are shown in Fig. 4(a). Here the strain energy calculated through Eq. (2) with geometry optimized by Keating potential is represented by the green squares, energy calculated with the accurate DFT method by black dots, and the Keating potential energy for the Keating-optimized optimized geometry by red rhombi. Our results show clearly that for Keating-optimized geometries, strain energies based on Eq. (2) reproduce our *ab initio* results rather well. On the other side, strain energies estimated using Keating potential alone not only significantly underestimates the strain, but also do not follow the correct general trend. This firmly establishes the applicability of the continuum methodology to polygonal nanotori under investigation.

For specific nanotori, local geometric features that are not described by Eq. (5) contribute to strain energy in addition to Eq. (11). Corresponding results are presented in Fig. 4(b). We considered a large set of polygonal nanotori, which were optimized by the Keating potential, and fitted a pair of torus radii (R, r) for each of them. We then correlated the strain energy ΔE_c^A obtained using the analytical expression in Eq. (11) with the more proper value $\Delta E_c^{Keating}$ based on the optimum discrete geometry, based on Eq. (2). As expected, most data points lie below the dashed $\Delta E_c^A = \Delta E_c^{Keating}$ line. Even though the strain energies estimated using the two approaches appear proportional to each other, it is clear that the analytical expression in Eq. (11) underestimates strain in polygonal nanotori significantly. We conclude that while a quick estimate of the strain energy based on Eq. (11)

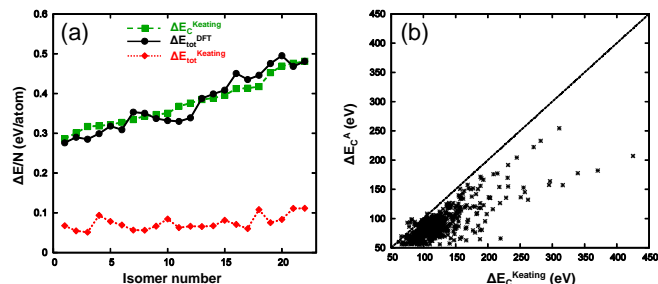


FIG. 4. (Color online) Strain energy ΔE in different polygonal nanotori. (a) Energy differences per atom ΔE_{tot}^{DFT} based on DFT and $\Delta E_{tot}^{Keating}$ based on the Keating potential are presented next to curvature energies $\Delta E_c^{Keating}$ based on Eq. (2) for Keating-optimized geometries. See the main text for detailed description. (b) Comparison between the analytical expression in Eq. (11) for the curvature energy ΔE_c^A based on the elastic description of a parametric torus and the curvature energy $\Delta E_c^{Keating}$ obtained using Eq. (2) for Keating-optimized discrete torus geometries.

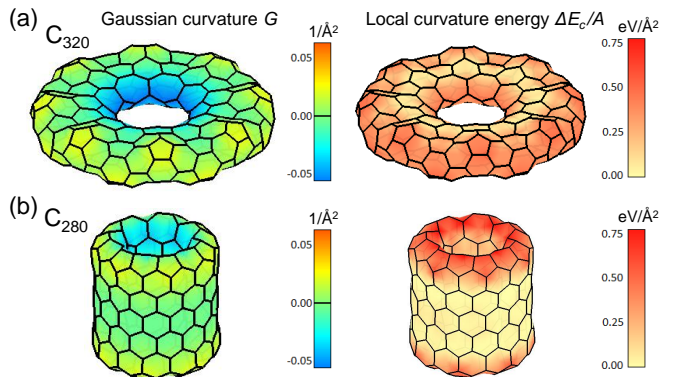


FIG. 5. (Color online) Local Gaussian curvature G (left panels) and local curvature energy $\Delta E_c/A$ (right panels) across the surface of selected nanotori. Representative examples shown are (a) the flattened C_{320} nanotorus with 320 atoms and (b) the elongated C_{280} nanotorus with 280 atoms. G and $\Delta E_c/A$ are interpolated from their values at the atomic sites.

is useful once the global parameters (R, r) are known, Eq. (2) should be used if quantitative comparison among different structures is intended.

LOCAL STABILITY ANALYSIS OF POLYGONAL NANOTORI

In the previous Section, we have considered nanotori as whole objects and established elasticity theory as a valid tool to estimate strain energy with respect to planar graphene in different torus isomers. The total strain energy ΔE , according to Eqs. (1),(2), (7), may be represented as an integral or a sum of local contributions. In other words, unlike in more complex DFT calculations, this approach allows to estimate local contributions towards the total strain energy. In the following, we will investigate the local strain distributions within individual nanotori. Next, we will apply this approach to analyze three series of polygonal nanotori and discuss trends in the strain energy in the light of a corresponding asymptotic analysis.

Local Curvature Distribution

The local geometry of a smooth, two-dimensional object may be characterized by two independent quantities, such as the local mean curvature k and the local Gaussian curvature G . These quantities can be used in Eq. (1) or its discretized counterpart, Eq. (2), to determine the curvature energy. The distribution of the local Gaussian curvature G_i and the local curvature energy per area, $\Delta E_c^{(i)}/A_0 = D[2k_i^2 - (1 - \alpha)G_i]$, across the surface of two representative nanotori is shown in Fig. 5.

In both cases, and others shown in the Supplemental

Material³⁷, the positively curved segments, shown in red in the left panels, are concentrated near the loci of pentagons along the outer perimeter. The negatively curved segments, shown in blue, are concentrated near the loci of heptagons along the inner perimeter. Specifically, the heptagons along the inner perimeter of the C_{320} nanotorus in Fig. 5(a) are well separated from the pentagons along the outer perimeter. This is different from the axially elongated C_{280} torus of Fig. 5(b), where pentagon-heptagon pairs at the upper and lower planes form an azulene-like pattern. As a consequence, the Gaussian curvature is more evenly distributed in the latter. We emphasize again that for closed nanotori, the summation of the local Gaussian curvatures is strictly zero as dictated by the Gauss-Bonnet theorem.

The distribution of the local curvature energy is even more intriguing. Within many nanotori we investigated, some of which are discussed in the Supplemental Material³⁷, we observed some degree of correlation between the absolute value of the local Gaussian curvature and the curvature energy. This should imply, at least for the nanotori investigated, that the two local curvatures k_i and G_i are not entirely independent. Yet the worth of this correlation has its limitations, as shown in Fig. 5. Whereas in the flattened C_{320} nanotorus in Fig. 5(a) the curvature energy is rather evenly distributed across the structure, the strain is clearly largest near the upper and lower ends of the C_{280} nanotorus in Fig. 5(b). This curvature energy distribution in the right panels differs obviously from the Gaussian curvature distribution in the left panels. The reason for this finding is that in these extreme structures, we can not truly decouple k_i and G_i . In C_{280} , $G_i \approx 0$ and k_i is constant in the central ‘tubular segments’. Only at the upper and lower ends, a large mean curvature k_i is required to connect the inner and the outer tube. The flatter C_{320} nanotorus lacks ‘tubular segments’ with $G_i \approx 0$. Therefore, the Gaussian curvature and curvature energy are better correlated and more evenly distributed in this isomer. The different shapes of carbon nanotori will be discussed in more detail later on.

We need to point out that the determination of the local Gaussian curvature G_i and the local mean curvature k_i is a non-trivial task that requires extra attention in discrete, irregular structures. According to the procedure outlined in Ref. 17, the determination of G_i requires second-nearest-neighbor information. On the other hand, the trivalency of graphitic carbon system lends itself to a compact definition of k_i based on nearest neighbors only. The asymmetry in handling the two curvatures leads to the possibility of negative local curvature energies according to Eq. (2), which is unphysical. This can be resolved by lowering the resolution of k_i , e.g. averaging its values using a window that also includes second-nearest neighbors.

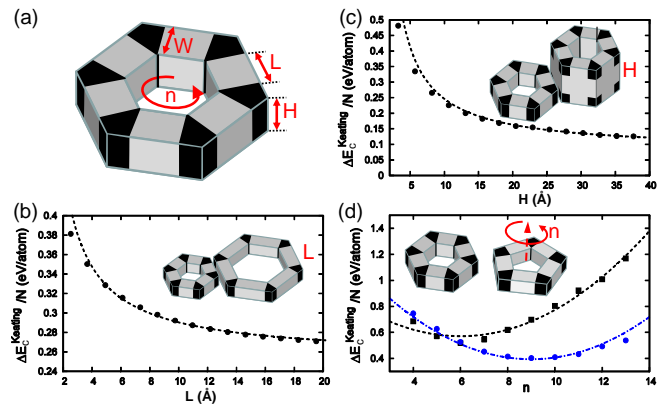


FIG. 6. (Color online) (a) A schematic model of a polygonal nanotorus with n -fold symmetry ($n = 6$ is shown here), consisting of n nanotube segments that are connected by n nanotube elbow joints. The nanotube segments are characterized by the width W , length L and height H . (b-d) Curvature energies per atom based on Eq. (2) for Keating-optimized nanotori of different shapes. ΔE_c is presented for nanotori with (b) $n, W, H = \text{const.}$, but nanotube length L changing, (c) $n, L, W = \text{const.}$, but nanotube height H changing, and (d) $L, W, H = \text{const.}$, but rotational symmetry number n changing. The insets show nanotorus models with different values of L , H and n . The lines in (b) and (c) are analytical extrapolations discussed in the text. Two sets of data points in (d), connected by lines to guide the eye, correspond to two structural families of nanotori, described in the text.

Shape Dependence of Stability

In spite of a large number of published reports^{34,35,38–46}, a systematic investigation of how the nanotorus stability depends on its shape has been missing. Here we intend to cover this gap by examining the dependence of the total curvature energy on main parameters defining the shape of polygonal carbon nanotori, namely the rotational symmetry number n , the length L and the width W of the nanotorus segments, and the height H of the nanotorus, shown schematically in Fig. 6(a). A more detailed classification scheme of polygonal nanotori is provided in References 28 and 47. In the following, we discuss the dependence of the curvature energy per atom ΔE_c on the shape parameters. The structures used to obtain the numerical results in Fig. 6(b-d) are displayed in the Supplemental Material³⁷, along with the distribution of local Gaussian curvature and curvature energy following the convention used in Fig. 5.

Side Length Dependence

We first look at an interesting case of a polygonal nanotorus consisting of n straight nanotube segments of finite length L that are connected by n elbow joints as illustrated in Fig. 6(a). As suggested in the insets of

Fig. 6(b), increasing the length of the nanotube segments reduces gradually the influence of the joints and for large L , the energy of the elbow joints becomes negligibly small when compared to the curvature energy of the straight tubular segments. This is illustrated for a specific family of nanotori in Fig. 6(b), where the data points represent results obtained using Eq. (2) for a set of Keating-optimized nanotori with different side length L that are displayed in the Supplemental Material³⁷.

For this particular series of nanotori, we may express the curvature energy per atom by $\Delta E_c(L)/N = a + b/L$ and display this dependence, with $a = 0.254$ eV and $b = 0.357$ eV·Å, by the dashed line in Fig. 6(b).

A more specific expression can be derived assuming that the nanotube segments are characterized by the chiral index (m, n) . In that case, the nanotube radius $r = 1.42 \text{ Å} \times \sqrt{m^2 + mn + n^2} \times \sqrt{3}/(2\pi)$ can be used in Eq. (12). For a nanotube segment of length L , the number of atoms can be estimated using $N = 2\pi r L/A_0$, where $A_0 = (1.42 \text{ Å})^2 \times 3\sqrt{3}/4 = 2.62 \text{ Å}^2$ is the area per atom in graphene. Then, we obtain

$$\frac{\Delta E_c(m, n)}{N} = A_0 \frac{\Delta E_c}{2\pi r L} = \frac{\sqrt{3}\pi^2 D}{2(m^2 + mn + n^2)}. \quad (13)$$

The nanotori in Fig. 6(b) are based on (4, 4) CNTs, yielding $\Delta E_c/N = 0.251$ eV, in very good agreement with the fitted constant a . The residual energy term b represents the local contribution from the elbow joints, which becomes negligibly small in the large L limit.

Height Dependence

Next, we study a series of polygonal nanotori resembling double-walled CNTs with their adjacent wall ends connected by a lip-lip interaction⁴ in the form of a graphitic network, shown in Fig. 6(c). With increasing height H of the nanotorus, the curvature energy per atom $\Delta E_c/N$ will be increasingly dominated by the central tubular part. In analogy to arguments used for nanotori with varying L , the total number of atoms N is proportional to H except a finite number at the double-wall nanotube ends. Then, the curvature energy per atom can be expressed by $\Delta E_c(H)/N = a' + b'/H$. This behavior, with the values $a' = 0.080$ eV and $b' = 1.658$ eV·Å, is reproduced by the dashed line in Fig. 6(c) for a particular series of nanotori depicted in the Supplemental Material³⁷.

Similar to the case discussed in Fig. 6(b), $\Delta E_c/N$ can be approximated by the sum of curvature energies of two nanotubes of length H , the inner one with radius r_i and the outer one with radius r_o . Then,

$$\begin{aligned} \frac{\Delta E_c(r_i, r_o)}{N} &= A_0 \frac{\Delta E_c(r_i) + \Delta E_c(r_o)}{2\pi(r_i + r_o)H} = \frac{A_0 D}{2r_i r_o} \quad (14) \\ &= \frac{\sqrt{3}\pi^2 D}{2\sqrt{(m_i^2 + m_i n_i + n_i^2)(m_o^2 + m_o n_o + n_o^2)}}. \end{aligned}$$

For the nanotori presented in Fig. 6(c), the chiral indices are $(m_i, n_i) = (5, 5)$ and $(m_o, n_o) = (10, 10)$, which gives the value $\Delta E_c/N = 0.080$ eV. This value, again, is in perfect agreement with the fitted value a' above. Again, the constant b' term describes the residual energy of the end joints connecting the inner and the outer tube.

In the above energy estimate, we have ignored the inter-layer interaction between the outer and inner wall. If the separation $r_o - r_i$ between the walls were as small as in graphite, this stabilizing interaction would reduce the strain energy by ≈ 0.03 eV/atom. In reality, a much smaller effect of this interaction is expected, since the strain at the end junctions tends to keep $r_o - r_i$ large and since the interaction should depend inversely on $(r_o - r_i)^6$. In any case, the inter-wall interaction is negligibly small in comparison to values shown in Fig. 6(c). In other, non-toroidal structures including helically coiled CNTs⁴⁸, the significance of the inter-wall interaction has to be accounted for on a case-by-case basis.

Rotational Symmetry Number Dependence

To the best of the authors' knowledge, all polygonal carbon nanotori investigated in the literature had rotational symmetry numbers $n = 5$ or $n = 6$. This is largely due to the fact that a nanotorus can be constructed in a cut-and-paste manner from graphene^{28,49,50} while preserving its original hexagonal symmetry. Also the majority of nanotori studied here has been constructed using a scheme generating isomers with either D_{nd} or D_{nh} point group symmetry. This constraint reduces greatly the number of possible isomers, but provides for an easy way to characterize individual polygonal nanotori by the relative positions of non-hexagonal rings within a rotational unit cell. With only selected results for $n = 5$ and $n = 6$ at hand, no conclusions are possible regarding the dependence of the stability on the rotational symmetry number.

Such results are presented in Fig. 6(d), where we display the curvature energy as a function of the rotational symmetry number, with n changing from $n = 4$ to $n = 13$, while all other shape parameters are fixed. We focus on two structural nanotori families. The first family, represented by black squares in Fig. 6(d), was studied more extensively in the literature^{13,34,35,51} and is found to be most stable for $n = 6$. The second family, represented by the blue dots, consists of a series of nanotori with a different distribution of non-hexagonal rings and is energetically optimal for $n = 9$ instead. The specific shapes of these two families are presented in the Supplemental Material³⁷.

Among the nanotori investigated in this study and shown in the Supplemental material³⁷, we find that a significant fraction minimized the curvature energy per atom for a non-hexagonal rotational symmetry. As a matter of fact, the distribution of 'optimum rotational symmetry numbers n_{opt} ', displayed in the Supplemental

tal Material³⁷, is roughly a Gaussian centered at $n_{opt} \approx 7$, with some extreme outliers at $n_{opt} = 12$. We found that the deviation of n_{opt} from the expected value $n_{opt} = 6$ is an artifact caused by the parametrized Keating force field, which is penalizing bond length deviations from 1.42 Å more than bond angle deviations from 120°, while underestimating the penalty for out-of-plane bending and thus somewhat distorting the optimum geometry.

The optimality of the $n = 6$ rotational symmetry number can be restored in the large-torus limit as follows. Let us consider a cut-and-paste model of a graphitic torus with $n = 6$ in the shape displayed in Fig. 6(a). It is clear that all non-hexagonal rings, which determine the angle $\varphi = 120^\circ$ between adjacent nanotube segments, will be located in the elbow joints colored in black, whereas the straight grey-colored segments will contain only hexagons. In large tori, the relative role of the elbow joints will play an ever diminishing role, and strain energy will be determined by the shape of the nanotube segments. Deviation from $n = 6$ will mean that the nanotube segments need to be bent, which causes extra strain.

CONCLUSIONS

We have presented comprehensive analysis on the elastic energy of carbon nanotori containing either only hexagons (polyhex nanotori) or also other polygons (polygonal nanotori) on the basis of continuum elasticity theory. In polyhex nanotori, we found that depending on the ratio between the major radius R and minor radius r of the torus, the in-plane and the out-of-plane contributions to the total elastic energy vary significantly. The wide CNT rings resembling nanotori, which have been observed experimentally, display only negligible in-plane strain, whereas the in-plane strain should exceed the out-of-plane strain for $R/r \lesssim 20$. In the polygonal nanotori studied here, the in-plane strain is rather small and the elastic energy obtained with the continuum method is shown to agree quantitatively with the results of *ab initio* DFT calculations. We also show that the analytical expression Eq. (11) can serve as a quick and qualitative reference for the elastic energy of nanotori once the shape

parameters (R, r) are known.

The capability of the current methodology is further demonstrated by a detailed analysis of the distributions of local excess energy in individual nanotori. Depending on the relative loci of non-hexagonal rings, the distribution of Gaussian curvature, mean curvature, and the local curvature energy can be either localized or evenly distributed across the nanotorus surface. This analysis can be extended to other 2D systems with different chemical composition and shape, and can also be related to the local stability and chemical reactivity index of different sites.^{17,52}

We have furthermore studied three different sets of polygonal nanotori with varying shape parameters, including the lateral and the axial dimension of the nanotori and the rotational symmetry number. Contrary to the common perception that the most stable nanotori all have a six-fold symmetry, we find that in smaller polygonal nanotori, the optimal rotational symmetry number covers a wide range $4 \lesssim n_{opt} \lesssim 12$. Only in the large-size limit, when the number of non-hexagonal defects is fixed, $n = 6$ emerges as the optimum rotational symmetry number. Asymptotic analysis on the variation of the other two shape parameters agrees quantitatively with the numerical results. This confirms that the current methodology, at least for the systems investigated here, is applicable across a wide length scale: From small nanotori where *ab initio* calculations are available, to mesoscopic tori, where continuum elasticity theory applies. Owing to the broad applicability, we believe that our approach will provide valuable results pertaining to the thermodynamical behavior of other large, experimentally observed carbon nanostructures, where atomic-scale treatment by *ab initio* techniques is not practical.

ACKNOWLEDGMENTS

This work was partly funded by the National Science Foundation Cooperative Agreement #EEC-0832785, titled “NSEC: Center for High-rate Nanomanufacturing”. Computational resources for this project were provided by the Michigan State University High-Performance Computer Center.

* tomanek@pa.msu.edu

¹ H. W. Kroto, J. R. Heath, S. C. O’Brien, R. F. Curl, and R. E. Smalley, *Nature* **318**, 162 (1985).

² S. Iijima, *Nature* **354**, 56 (1991).

³ K. S. Novoselov, A. K. Geim, S. V. Morozov, D. Jiang, Y. Zhang, S. V. Dubonos, I. V. Grigorieva, and A. A. Firsov, *Science* **306**, 666 (2004).

⁴ D. Tománek, *Guide Through the Nanocarbon Jungle*, 2053-2571 (IOP Publishing, Bristol, UK, 2014).

⁵ M. S. Dresselhaus, G. Dresselhaus, and P. Avouris, *Carbon Nanotubes: Synthesis, Structure, Properties, and Applica-*

tions (Springer, Berlin, Germany, 2001).

⁶ L. Liu and J. Zhao, in *Syntheses and Applications of Carbon Nanotubes and Their Composites*, edited by S. Suzuki (InTech, Rijeka, Croatia, 2013).

⁷ M. Zheng and C. Ke, *Small* **6**, 1647 (2010).

⁸ L. Chen, H. Wang, J. Xu, X. Shen, L. Yao, L. Zhu, Z. Zeng, H. Zhang, and H. Chen, *J. Am. Chem. Soc.* **133**, 9654 (2011).

⁹ L. Liu, G. Y. Guo, C. S. Jayanthi, and S. Y. Wu, *Phys. Rev. Lett.* **88**, 217206 (2002).

¹⁰ M.-F. Lin, *J. Phys. Soc. Jpn.* **67**, 1094 (1998).

- ¹¹ M. F. Lin and D. S. Chuu, *Phys. Rev. B* **57**, 6731 (1998).
- ¹² C. G. Rocha, M. Pacheco, Z. Barticevic, and A. Latgé, *Phys. Rev. B* **70**, 233402 (2004).
- ¹³ A. Ceulemans, L. F. Chibotaru, and P. W. Fowler, *Phys. Rev. Lett.* **80**, 1861 (1998).
- ¹⁴ T. A. Hilder and J. M. Hill, *Phys. Rev. B* **75**, 125415 (2007).
- ¹⁵ M. T. Lusk and N. Hamm, *Phys. Rev. B* **76**, 125422 (2007).
- ¹⁶ N. Hamada, S.-i. Sawada, and A. Oshiyama, *Phys. Rev. Lett.* **68**, 1579 (1992).
- ¹⁷ J. Guan, Z. Jin, Z. Zhu, C. Chuang, B.-Y. Jin, and D. Tománek, *Phys. Rev. B* **90**, 245403 (2014).
- ¹⁸ L. D. Landau, L. P. Pitaevskii, A. M. Kosevich, and E. M. Lifshitz, *Theory of Elasticity, Third Edition: Volume 7 (Course of Theoretical Physics)* (Pergamon Press, London, England, 1959).
- ¹⁹ P. N. Keating, *Phys. Rev.* **145**, 637 (1966).
- ²⁰ E. Artacho, E. Anglada, O. Dieguez, J. D. Gale, A. Garcia, J. Junquera, R. M. Martin, P. Ordejon, J. M. Pruneda, D. Sanchez-Portal, and J. M. Soler, *J. Phys. Cond. Mat.* **20**, 064208 (2008).
- ²¹ D. M. Ceperley and B. J. Alder, *Phys. Rev. Lett.* **45**, 566 (1980).
- ²² J. P. Perdew and A. Zunger, *Phys. Rev. B* **23**, 5048 (1981).
- ²³ N. Troullier and J. L. Martins, *Phys. Rev. B* **43**, 1993 (1991).
- ²⁴ H. J. Monkhorst and J. D. Pack, *Phys. Rev. B* **13**, 5188 (1976).
- ²⁵ M. R. Hestenes and E. Stiefel, *J. Res. Natl. Bur. Stand.* **49**, 409 (1952).
- ²⁶ G. Overney, W. Zhong, and D. Tomanek, *Z. Phys D: Atoms, Molecules and Clusters* **27**, 93 (1993).
- ²⁷ C. Q. Ru, *Phys. Rev. B* **62**, 9973 (2000).
- ²⁸ C. Chuang, Y.-C. Fan, and B.-Y. Jin, *J. Chem. Inf. Model.* **49**, 361 (2009).
- ²⁹ O. Hod, E. Rabani, and R. Baer, *Phys. Rev. B* **67**, 195408 (2003).
- ³⁰ M. Ahlskog, E. Seynaeve, R. Vullers, C. Van Haesendonck, A. Fonseca, K. Hernadi, and J. B Nagy, *Chem. Phys. Lett.* **300**, 202 (1999).
- ³¹ R. Martel, H. R. Shea, and P. Avouris, *Nature* **398**, 299 (1999).
- ³² L. Song, L. J. Ci, L. F. Sun, C. Jin, L. Liu, W. Ma, D. Liu, X. Zhao, S. Luo, Z. Zhang, Y. Xiang, J. Zhou, W. Zhou, Y. Ding, Z. L. Wang, and S. Xie, *Advanced Materials* **18**, 1817 (2006).
- ³³ C. R. Chang, L. H. Lu, J. H. Liu, and W. Chen, *Chem. Phys.* **393**, 123 (2012).
- ³⁴ J. E. Avron and J. Berger, *Phys. Rev. A* **51**, 1146 (1995).
- ³⁵ J. Berger and J. E. Avron, *J. Chem. Soc., Faraday Trans.* **91**, 4037 (1995).
- ³⁶ R. Martel, H. R. Shea, and P. Avouris, *J. Phys. Chem. B* **103**, 7551 (1999).
- ³⁷ See Supplemental Material at <http://link.aps.org/supplemental/10.1103/PhysRevB.000.000000> for optimum geometries, local Gaussian curvature and local strain distribution in nanotori with different shape parameters.
- ³⁸ B. I. Dunlap, *Phys. Rev. B* **50**, 8134 (1994).
- ³⁹ B. I. Dunlap, *Phys. Rev. B* **46**, 1933 (1992).
- ⁴⁰ S. Itoh, S. Ihara, and J.-I. Kitakami, *Phys. Rev. B* **47**, 1703 (1993).
- ⁴¹ S. Ihara, S. Itoh, and J.-I. Kitakami, *Phys. Rev. B* **47**, 12908 (1993).
- ⁴² S. Itoh and S. Ihara, *Phys. Rev. B* **48**, 8323 (1993).
- ⁴³ S. Itoh and S. Ihara, *Phys. Rev. B* **49**, 13970 (1994).
- ⁴⁴ S. Ihara, S. Itoh, K. Akagi, R. Tamura, and M. Tsukada, *Phys. Rev. B* **54**, 14713 (1996).
- ⁴⁵ R. Setton and N. Setton, *Carbon* **35**, 497 (1997).
- ⁴⁶ I. László and A. Rassat, *J. Chem. Inf. Comput. Sci.* **43**, 519 (2003).
- ⁴⁷ C. Chuang, Y.-C. Fan, and B.-Y. Jin, *J. Chem. Inf. Model.* **49**, 1679 (2009).
- ⁴⁸ C. Chuang, Y.-C. Fan, and B.-Y. Jin, *J. Mol. Struct.* **1008**, 1 (2012).
- ⁴⁹ R. Tamura, M. Ikuta, T. Hirahara, and M. Tsukada, *Phys. Rev. B* **71**, 045418 (2005).
- ⁵⁰ F. Beuerle, C. Herrmann, A. C. Whalley, C. Valente, A. Gamburd, M. A. Ratner, and J. F. Stoddart, *Chemistry: A European Journal* **17**, 3868 (2011).
- ⁵¹ M. T. Lusk and N. Hamm, *Phys. Rev. B* **76**, 125422 (2007).
- ⁵² A. A. Pacheco Sanjuan, M. Mehboudi, E. O. Harriss, H. Terrones, and S. Barraza-Lopez, *ACS Nano* **8**, 1136 (2014).